# Dynamic Characteristics of a Tool Holder Shank in Lathe

**Carry Andersson**

**Lennart Kisswani**

Department of Mechanical Engineering

University of Karlskrona/Ronneby

Karlskrona, Sweden

2000

Thesis submitted for completion of Master of Science in Mechanical Engineering with emphasis on Structural Mechanics at the Department of Mechanical Engineering, University of Karlskrona/Ronneby, Karlskrona, Sweden.

**Abstract:**
Dynamic characteristics of a Tool Holder Shank were determined by using the Finite Element Method and Experimental Modal Analysis. Good agreement between FE-model and the experimental model was obtained for the Tool Holder Shank itself. With the Tool Holder Shank in Lathe the agreement was less good. Reasons for this are discussed. Suggestions for further work on including actuators to reduce vibrations are given.

**Keywords:**
Dynamic Characteristics, Tool Holder Shank, Lathe, Turning, Actuators, FE-model, Modal Analysis, Experimental Verification.

# Acknowledgements

This work was carried out at the Department of Mechanical Engineering, University of Karlskrona/Ronneby, Karlskrona, Sweden, under the supervision of Dr Mats Walter. We wish to express our sincere appreciation for his guidance throughout the work.

The work was initiated in July 1999 as a co-operation project between the Department of Telecommunications and Signal Processing and the Department of Mechanical Engineering at the University of Karlskrona/Ronneby.

We also wish to express our sincere appreciation to Dr Lars Håkansson at the Department of Telecommunications and Signal Processing who acted as a co-supervisor, as well as the whole department for their help and support throughout the work.

Finally, we would like to thank our colleagues in the Master of Science programme and all the members of the Department of Mechanical Engineering for valuable discussions and support.

Karlskrona, February 2000

*Carry Andersson*

*Lennart Kisswani*

# Contents

# 1. Notation

| | |
|---|---|
| $\mathbf{I}$ | Identity matrix |
| $\mathbf{K}$ | Stiffness matrix [N/m] |
| $\mathbf{M}$ | Mass matrix [kg] |
| $\mathbf{U}$ | Mass normalised eigenvectors |
| $\overline{\mathbf{K}}$ | Shifted stiffness matrix [N/m] |
| $F$ | Input force signal |
| $H$ | Transfer function |
| $K$ | Stiffness matrix [N/m] |
| $L$ | Length [m] |
| $M$ | Moment [Nm] |
| $X$ | Output signal |
| $\mathbf{r}$ | Starting vector |
| $\mathbf{u}$ | Mode shape vector [m] |
| $\mathbf{x}$ | Displacement vector [m] |
| $c$ | Damping constant |
| $f$ | Frequency [Hz] |
| $i$ | Number |
| $j$ | Imaginary unit, number |
| $k$ | Stiffness [N/m] |
| $m$ | Mass [kg] |
| $n$ | Number |
| $s$ | Transform variable, feed rate [mm/rev] |
| $t$ | Time [s] |
| $u$ | Eigenvector |
| $v$ | Velocity [m/s] |
| $x$ | Displacement [m], co-ordinate direction |
| $y$ | Co-ordinate direction |
| $z$ | Co-ordinate direction |
| $\gamma^2$ | Coherence function |
| $\lambda$ | Eigenvalue |
| $\overline{\lambda}$ | Eigenvalues of shifted problem |
| $\sigma$ | Eigenvalue shift |
| $\omega$ | Natural frequency [Hz] |
| $S_{xx}$ | Power spectral density of the signal $x$ [dB] |

| | |
|---|---|
| $S_{xy}$ | Cross spectral density of the signal $x$ and the signal $y$ [dB] |
| $S_{yx}$ | Cross spectral density of the signal $y$ and the signal $x$ [dB] |
| $S_{yy}$ | Power spectral density of the signal $y$ [dB] |

## Indices

| | |
|---|---|
| $_T$ | Transpose |
| $_t$ | Tightening |
| $_n$ | Number |
| $_i$ | Number |
| $_j$ | Imaginary unit, number |
| $_x$ | Signal, input |
| $_y$ | Signal, output |
| $_{dr}$ | Damped natural frequency |
| $_{lin}$ | Linear |

## Abbreviations

| | |
|---|---|
| EMA | Experimental Modal Analysis |
| FEM | Finite Element Method |
| FRF | Frequency Response Function |
| MDOF | Multiple Degree of Freedom |
| SVI | Simultaneous Vector Iteration |

# 2 Introduction

## 2.1 Background

The turning process is one of the most important manufacturing processes in the industry today. The evolution of the turning process has been ongoing in the last centuries. It can be seen as a part of the industrial evolution. Every day, we use turned products, from the hardware to deliver water to kitchen faucets, cars and planes for transportation, furniture and so on, see figure 2.1. Over the past thirty years, new technologies have made a dramatic impact on the turning process. The new technologies have made it possible to produce goods of better quality, faster and at lower costs. Examples are the numeric controlled machines that make it possible to manufacture a complex work piece in one single operation.

In modern turning industry one of most important factors to obtain high productivity and high quality is production safety. Factors that affect the production safety are among others durability of the lathe, tool life and also the machinability of the workpiece material. The machinability, or cuttability, can be quantified from the cutting power or cutting forces that the work piece give rise to, how easy chip breakage is obtained, the work piece material influence of the tool life and finally the surface finish of the machined product. These different aspects usually interact, e.g. a work piece where it is easy to obtain fair surface finish, usually gives rise to high cutting forces. There are many process behaviours that affect the surface finish, e.g. the ability to get build-up edges or layers and the cutting forces themselves. Both the mean values of the cutting forces and the dynamic properties influence the surface finish. The dynamic characteristics give rise to vibrations in the lathe and the work piece.

*Figure 2.1. Examples of different turned products.*

Generally in turning operations there will be some level of relative dynamic motion between cutting tool and work piece. Energy from the chip formation process excites the mechanical modes of the machine-tool system. Modes of the work piece may also influence tool vibration. The dynamic properties of the excitation, i.e. the chip formation process are correlated to the material properties and the geometry of the work piece. The vibrations may lead to unwanted noise, degraded surface finish and reduced tool life.

## 2.2 Project Description

A common way to avoid vibration problem is to operate the turning process under-critical and thereby reduce the excitation of the modes of the machine-tool system and/or the work piece. However, under-critical turning process will often lead to high manufacturing and operation time. One way to reduce the vibration problem associated with critical machining is to use actuators, which automatically modifies the structural response of the tool holder shank, which leads to further reduction of the dynamic motion between cutting tool and work piece. This leads to turning products with higher cutting data that results in a reduction of the production time and hence competitive products.

The aim of this work is to determine the natural frequencies, mode shapes and damping ratios for a Tool Holder Shank. This is a first step in investigating if it would be possible to use piezoelectric actuators to reduce vibrations during the cutting process.

## 2.3 Method

The first step is to develop a mathematical model using the Finite Element Method (FE-model) of the problem to get an understanding of the dynamics involved. To verify the FE-model an Experimental Modal Analysis (EMA) is done. Based on the experimental results the FE-model is adjusted and when the FE-model and the experimental model correlates accurately the FE-model of the tool holder shank is accepted.

The agreement between FE-models and the experimental models gives opportunity to use the FE-models for more extensive studies without further extensive experimental measurements.

# 3 Theories

## 3.1 Turning

### 3.1.1 The Turning Operation

Turning [2] in its simplest form is a machining process used to generate external, cylindrical surfaces by removing material by a cutting tool. The primary motion is rotation. The feed motion is normally a rectilinear movement, see figure 3.1. When machining, the work piece is perpendicular to the cutting tool.

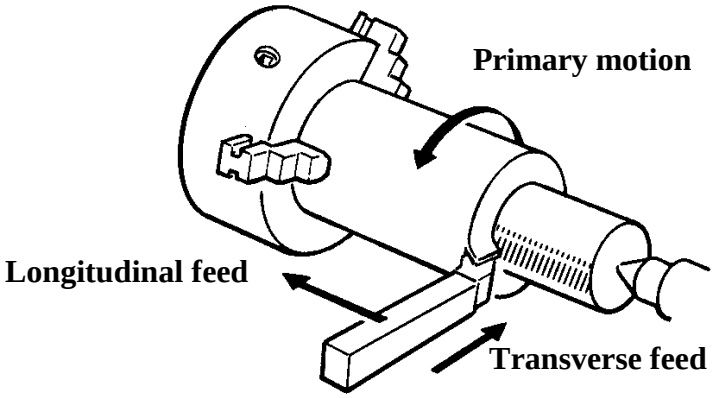


*Figure 3.1. The external longitudinal turning process [2].*

### 3.1.2 Undesired Vibrations and Noise

Undesired vibrations are a serious problem that affects and deteriorates the surface finish of the work piece. It also affects the dimensional accuracy of the work piece, and reduces tool/machine lifetime. Also vibrations can be initiated in machine tools by component defects, unbalanced parts, poor assembly etc.

One way to represent the vibration energy in a cutting process [6] is to plot the cutting speed as a function of frequency, see figure 3.2.

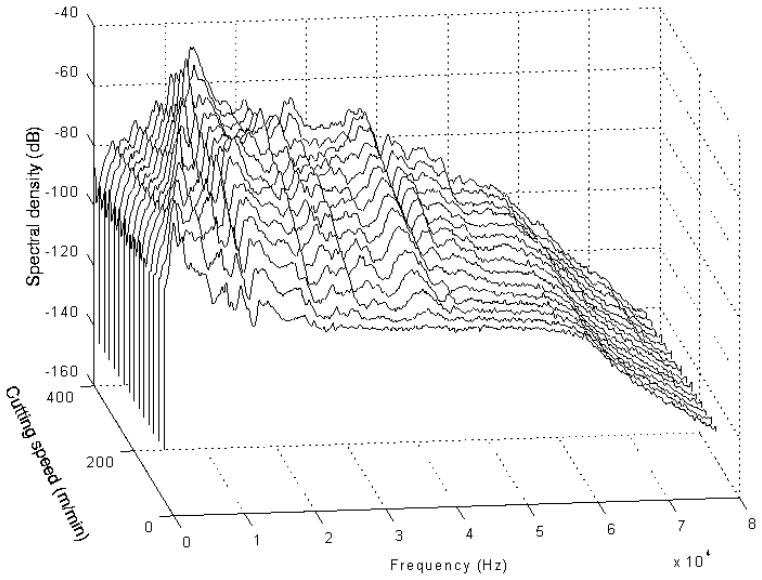


*Figure 3.2. Typical spectral density estimate of the dynamic response for a tool holder shank in the primary direction during a continuous cutting operation in SS0727-02 with constant feed rate s = 0.5 mm/rev and cutting speed v = 50 – 400 m/min [6].*

To show that the natural frequencies are constant at each feed rate and cutting speed the spectral density is plotted for cutting speed from 50 - 400 m/min. Figure 3.2 also shows the dynamic response in the primary direction during a continuous cutting operation.

Other problems in machining are plastic deformation and friction in the contact between the cutting tool and the work piece. This contact generates heat, which increases the temperature of both components, see figure 3.3. The elevated temperature of the tool reduces its wear resistance and changes both the geometry and the size of the turned component. If the vibrations are controlled, higher cutting data can be used and the time varying loads on the cutting tool are decreased. The result is longer tool/machine lifetime.

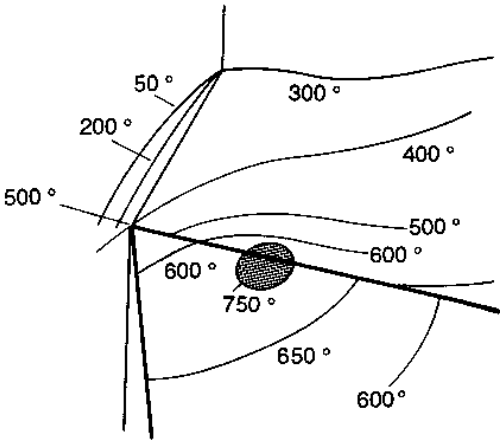


*Figure 3.3. Temperature distribution in the cutting area [2].*

If the working environment is considered, noise is frequently introduced by dynamic motion between the cutting tool and the work piece. By improving the dynamic stiffness of the machine structure, the problem of relative dynamic motion between cutting tool and work piece may be partially solved.

## 3.2 Actuators

Reducing the noise and the undesired vibrations is clearly a very important goal. This can be achieved by using actuators, which automatically modifies the structural response of a mechanical system. The actuator is used to enhance the performance of a structural system by inducing a favourable structural deformation according to the applied voltage. It develops cancelling force to reduce the vibration level and acoustic noise level. There are several types of actuators that could be used to solve vibration problems in mechanical systems, for example magnetostrictive [1] and piezoelectric actuators [11]. Typical application areas for actuators are flexible robotics, aircraft, marine hulls, vibrating machinery and modal testing. In control applications piezoelectric actuators are usually preferred due to their superior linearity and simplicity to mount on the structures to be controlled. In our application the selection of actuator type is limited to the

piezoelectric actuators by two facts; the actuator mount and the linearity request.

### 3.2.1 Piezoelectric Actuators

The “patch” actuator [10] is a piezoelectric actuator containing a high efficiency piezoceramic element within a rugged, electrically insulated housing, see figure 3.4. It has an integral cable and is attached to the structure with a two-part epoxy or similar adhesive.

*Figure 3.4. “Patch” actuators [10].*

Actuators convert electrical signals like voltages or charges into mechanical displacements or forces. As for sensors, a reasonably linear relationship between input signal and movement is required the actuators can be divided in three main groups.

- Axial actuators
- Transversal actuators
- Flexural actuators

Axial and transversal actuators have high stiffness and are optimised for small movements and high forces. Flexural actuators cover the applications where larger movements are required. However, they have a restricted ability withstand large stress, and are usually used on light structures. Advantages of piezoelectric actuators is their low profile, low mass and high output, it makes the actuator ideal for controlling adaptive structures.

## 3.3 Dynamics

### 3.3.1 Multiple Degree of Freedom (MDOF) Systems

Figure 3.5 illustrates an undamped system with *n* translation degrees of freedom.

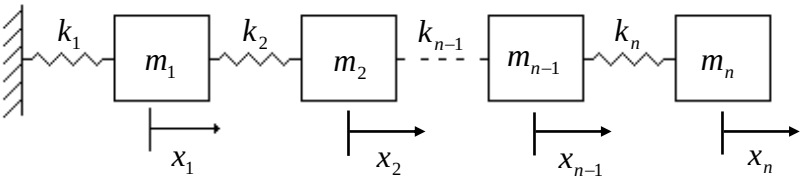


*Figure 3.5. Undamped MDOF-system.*

The forces from the springs acting on each mass are determined through a free body diagram, see figure 3.6.

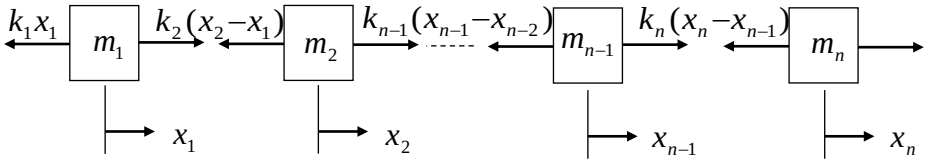


*Figure 3.6. Free body diagram for the undamped MDOF-system.*

Using Newton's second law equations of motion for each mass can be written as

$$
\begin{aligned}
&m_1\ddot{x}_1 + x_1(k_1+k_2) - x_2k_2 = 0\\
&m_2\ddot{x}_2 + x_2(k_2+k_3) - k_2x_1 - k_3x_3 = 0\\
&\vdots\\
&m_{n-1}\ddot{x}_{n-1} + x_{n-1}(k_{n-1}+k_n) - k_nx_n - k_{n-1}x_{n-1} = 0\\
&m_n\ddot{x}_n - k_nx_{n-1} + k_nx_n = 0
\end{aligned}
\qquad (3.1)
$$

Equation 3.1 consists of *n* coupled second order differential equation and can be written in matrix form as

$$\mathbf{M}\ddot{\mathbf{x}} + \mathbf{K}\mathbf{x} = 0 \tag{3.2}$$

where **M** is the mass matrix and **K** is the stiffness matrix, and **x** is the displacement vector. Dots indicate time derivatives.

### 3.3.2 Natural Frequencies and Mode Shapes

Assuming harmonic motion for the spring-mass system [7] the displacements are expressed as

$$\mathbf{x}(t) = \mathbf{u}e^{j\omega t} \tag{3.3}$$

where **u** is a vector of amplitudes and $\omega$ is the natural angular frequency. Substituting this into the equations of motion yields

$$(-\omega^2\mathbf{M} + \mathbf{K})\mathbf{u}e^{j\omega t} = 0 \tag{3.4}$$

Noting that the scalar $e^{j\omega t} \neq 0$ for any value of *t* equation 3.4 yields that

$$(-\mathbf{M}\omega^2 + \mathbf{K})\mathbf{u} = 0 \tag{3.5}$$

Equation (3.5) is a generalised eigenvalue problem and has non trivial solutions if

$$\det(-\omega^2\mathbf{M} + \mathbf{K}) = 0 \tag{3.6}$$

This is called the *characteristic equation* of the system and has solutions $\omega_1^2, \omega_2^2, ..., \omega_n^2$, known as the eigenvalues. The eigenvalues give the natural frequencies. For the eigenvalues the corresponding eigenvectors $u_1, u_2, ..., u_n$ can be obtained. The eigenvectors describe the mode shapes of the dynamic system.

## 3.4 Modal Analysis

Modal analysis theory [8] refers to classical vibration theory that explains, theoretically, the existence of natural frequencies, damping ratios and mode shapes for linear systems. This theory includes lumped-parameter or discrete models as well as continuos models. The theory also includes real

normal modes as well as complex modes of vibration as possible solutions for the modal parameters.

Modal analysis is used to help design the structural system for noise and vibration applications.

The modes of a structure or system can be estimated from two different approaches:

- Mathematical Models
- Experimental Modal Analysis

### 3.4.1 Mathematical Models

In its most basic form, a mathematical model simplifies a structure by breaking it up into masses and springs. This process can be done by the simple lumped mass and lumped spring approach. This modelling process reduces the complicated structure into many mass/spring systems. The eigenvalue problem can then be solved to get the frequency and mode shape of each mode for the assumed mass and stiffness distribution. When the modes are established, calculations can be done to determine how the structure will respond to various dynamic inputs. One of the forced response runs that is often used is to input a unit force with variable frequency at one point while monitoring the response as a function of frequency (FRF) at several important locations.

### 3.4.2 Experimental Modal Analysis

Experimental Modal Analysis (EMA) is the interpretation of test data collected from a vibrating structure [8]. It involves determining modal parameters as frequencies, damping ratios, and mode shapes of a linear time-invariant system. A common reason for EMA is verification of results from FE-models.

## 3.5 Eigenvalues and Eigenvectors in I-DEAS

For FE-calculations of the natural frequencies and modeshapes I-DEAS System Dynamics Analysis software is used. There are several ways of determining the eigenvalues and eigenvectors when calculating the natural frequencies and modeshapes. In our case the Lanczos method [5] is used due to its many advantages in comparison to the other methods, Guyan, and SVI.

### 3.5.1 Lanczos Formulation

The purpose of the Lanczos method is to compute a relatively few eigenvalue and eigenvector pairs for a model defined by a large number of degrees of freedom. By using restart solutions coupled with frequency shifting, a large number of modes can be determined efficiently by obtaining a few at a time.

The technique can be used to solve certain large, sparse, symmetric eigenproblems. The method involves partial tridiagonalisations of the given matrix. Information about extremal eigenvalues tends to emerge long before the tridiagonalisation is complete. This makes the Lanczos algorithm particularly useful in situations where a few of the largest or smallest eigenvalues are desired.

### 3.5.2 Lanczos Algorithm

The Lanczos algorithm [5] has the ability to compute the smaller eigenvalues of a matrix without any factorisation. However, they will not be approximated accurately until nearly all eigenvalues have been determined. Consequently, it is necessary to apply Lanczos factorisation to an inverted form of the matrix.

The Lanczos algorithm uses a shift-and-invert procedure to converge quickly to the eigenvalues closest to the shift. The eigenvectors of the original and shifted problem are the same. The general eigenproblem is

$$\mathbf{Kx} = \lambda\mathbf{Mx} \tag{3.7}$$

Frequency shifting selectively extract modes by shifting the analysis, so that mode extraction begins at higher modes or higher frequencies. Frequency shifting shifts the eigenvalue problem so that the lowest eigenvalues are closest to the frequency shift point. Applying a shift, the algorithm works with the equation

$$\overline{\mathbf{K}}\mathbf{x} = \overline{\lambda}\mathbf{M}\mathbf{x} \tag{3.8}$$

where

$$\overline{\mathbf{K}} = \mathbf{K} - \sigma\mathbf{M} \tag{3.9}$$

Since the algorithm works with the inverse of $\overline{\mathbf{K}}$ the spectrum of the original eigenproblem is related to the spectrum of the shifted problem by

$$\lambda = \frac{1}{\overline{\lambda} - \sigma} \tag{3.10}$$

The Lanczos method constructs an orthogonal set of vectors, known as Lanczos vectors, for use in the Rayleigh-Ritz [3] procedure. Given a starting vector **r**, these basic methods generates a sequence of vectors

$$\left\{\mathbf{r}, \overline{\mathbf{K}}^{-1}\mathbf{M}\mathbf{r}, \left(\overline{\mathbf{K}}^{-1}\mathbf{M}\right)2\mathbf{r}, ....., \left(\overline{\mathbf{K}}^{-1}\mathbf{M}\right)j\mathbf{r}\right\} \tag{3.11}$$

during *j* iterations. These vectors are referred to as the Krylov sequence [5]. The sequence converges (as $j \rightarrow$ infinity) to the eigenvector corresponding to the eigenvalue closest to the shift.

The basic difference between the Lanczos method and the other two methods (Guyan, and SVI) is that the information contained in each successive vector of the Krylov sequence is used to obtain the best approximation to the wanted eigenvectors instead of using only the last vector in the sequence. In other words, the Lanczos algorithm is equivalent to obtaining the Rayleigh-Ritz approximation with the vectors in the Krylov sequence as the trial vectors.

This method involves supplementing the Krylov sequence with an orthogonalisation process with respect to the other vectors. The result is a set of M-orthonormal vectors (the Lanczos vectors) that is used in the Rayleigh-Ritz procedure to reduce the dimension of the eigenproblem. This leads to a standard eigenproblem with a tri-diagonal matrix.

## 3.6 Signal Processing and Vibration Testing

### 3.6.1 Transfer Functions used in Vibration Measurement

Usually vibration is measured in terms of motion and therefore the corresponding frequency response function may be presented in terms of displacement, velocity or acceleration, see table 3.1.

*Table 3.1. Transfer functions.*

| Response Measurement | Transfer Function | Inverse Transfer Function |
|---|---|---|
| Acceleration | Accelerance | Apparent mass |
| Velocity | Mobility | Impedance |
| Displacement | Receptance | Dynamic stiffness |

The three transfer functions given in Table 3.1 are related to each other by simple multiplications of the transform variable *s*, since this corresponds to differentiation. Thus with the *receptance transfer function* denoted by

$$\frac{X(s)}{F(s)} = H(s) = \frac{1}{ms^2 + cs + k} \tag{3.12}$$

the *mobility transfer function* becomes

$$\frac{sX(s)}{F(s)} = sH(s) = \frac{s}{ms^2 + cs + k} \tag{3.13}$$

because *sX(s)* is the transform of the velocity. Similarly, $s^2X(s)$ is the transform of the acceleration and the *accelerance transfer function* becomes

$$\frac{s^2X(s)}{F(s)} = s^2H(s) = \frac{s^2}{ms^2 + cs + k} \tag{3.14}$$

Each of these also defines the corresponding frequency response function by substituting $s = j\omega_{dr}$.

For example, the response measurements done in Chapter 5 are made by using accelerometers and by using laser vibrometer. The accelerometers measure the acceleration in a certain point giving the corresponding accelerance transfer function. The laser vibrometer on the other hand measures the velocity in a certain point giving the corresponding mobility transfer function. To be able to compare the results the transform variable *s* has to be used according to equation 3.13 and 3.14. The accelerance transfer function, Equation 3.14, could by divided by *s* or the mobility transfer function, Equation 3.13, could be multiplied by *s*.

### 3.6.2 Coherence

The coherence function, denoted by $\gamma^2$, is defined to be the ratio of the two values of the frequency response function *H(jω)*, calculated from the equations below:

$$S_{yx}(\omega) = H(j\omega)S_{yy}(\omega) \tag{3.15}$$

$$S_{xx}(\omega) = H(j\omega)S_{xy}(\omega) \tag{3.16}$$

where $S_{yx}(\omega)$ and $S_{xy}(\omega)$ is the cross-spectral density [9] of the signal *x(t)* and the signal *y(t)*, $S_{xx}(\omega)$ and $S_{yy}(\omega)$ is the power spectral density [9] of each signal. This yields

$$\gamma^2 = \frac{\left|S_{xy}(\omega)\right|^2}{S_{xx}(\omega)S_{yy}(\omega)} \tag{3.17}$$

The coherence function gives a measure of how well the output signal corresponds linearly to the input signal at a specific frequency. The value of the coherence function always lies between zero and unity, see Figure 3.7. If the output signal can be explained linearly from the input signal the coherence is unity. If the output signal is statistically independent or nonlinearly related to the input signal the coherence is zero.

The coherence is taken as an indication of how accurate the measurement process is over a given range of frequencies.

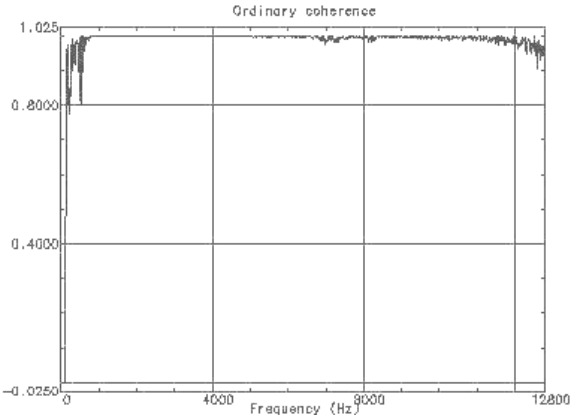


*Figure 3.7. Example of a coherence function.*

Values close to unity should occur near the structure's resonance frequencies. At resonance the signals are large and less affected by noise. Usually data with a coherence of less than 0.9 indicates that the test should be redone.

## 3.7 Correlation

There are several ways of determining how closely the experimental and analytical models correspond. Several comparison techniques are presented in [8]. In general comparison techniques are to a greater or lesser extent based on the orthogonality conditions:

$$\mathbf{U}^{\mathbf{T}}\mathbf{M}\mathbf{U} = \mathbf{I} \qquad \text{and} \qquad \mathbf{U}^{\mathbf{T}}\mathbf{K}\mathbf{U} = \left[\omega_n^2\right] \tag{3.18}$$

where **U** represents the mass normalised eigenvectors, either from test or analysis, and **I** and $[\omega_n^2]$ are the diagonal identity and eigenvalue matrices, respectively.

### 3.7.1 Comparison of Natural Frequencies

One way to compare the natural frequencies for a predicted and experimental model is to plot the experimental values against the predicted values [4]. In this way it is possible to see the degree of correlation between

the two sets of results. The points plotted should lie on or close to a straight line, see figure 3.8.


*Figure 3.8. Example of comparison of measured and predicted natural frequencies.*

### 3.7.2 Comparison of Mode Shapes

One way to compare the mode shapes for a predicted and experimental model is to plot the predicted and experimental nodal amplitudes as indicated in figure 3.9. The individual points on this plot relate to specific co-ordinates on the model and should lie close to a straight line passing through the origin.

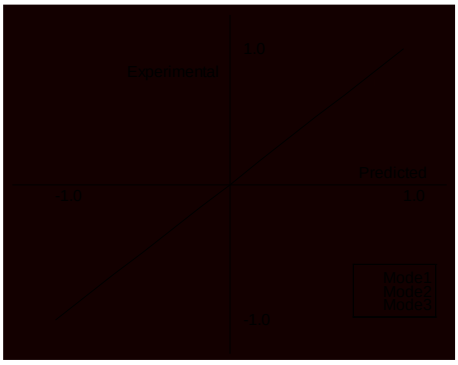


*Figure 3.9. Example of comparison of measured and predicted mode shapes.*

# 4 Theoretical Models

## 4.1 Elements

One of the most important choices when making a finite element model is which element type to use. There is three different types presented here. The beam element, shell element and solid element. All finite element modelling is performed in I-DEAS.

### 4.1.1 Beam Elements

Beam elements can be used to make a very efficient finite element model to predict overall deflection and bending moments but will not be able to predict the local stress concentrations at the point of application of a load or at joints. One of the advantages of using beam elements is that the computer time is relatively short since it has fewer degrees of freedom. A beam has three transitional degrees of freedom and three rotational degrees of freedom. There are four types of beam elements in I-DEAS: linear, parabolic, curved, and tapered.

### 4.1.2 Shell Elements

Shell elements can be effectively used for structures with relatively thin walls such as sheet metal parts, discs, plates, etc.

### 4.1.3 Solid Elements

The most general elements are the solid elements. The disadvantage is that more elements and nodes are usually required, and the model will therefore be more time demanding to solve, compared to for example a beam element model. However, many devices designed by engineers have highly three-dimensional geometry, which makes it necessary to use three-dimensional elements.

## 4.2. Boundary Conditions

It is very important to understand how the boundary condition is defined. The boundary condition includes loads, temperature restraints, and displacement restraints. It is also very important that especially the experimental set-up is well defined and experimental repeatable. Exact definition of the boundary conditions may be problematic, but nevertheless, tests should be considered to prove the repeatability of the installation.

### 4.2.1 Free-Free

For a structure to be really free, it should be suspended in the air, free in space with no holding points whatsoever. Such a situation is commonly designated as free-free. The simulation of free-free conditions is easy to achieve. It suffices to suspend or support the structure using very flexible springs so that the rigid body resonance frequencies are far away from the frequency range of interest. In this work rubber bands were used, see figure 5.2.

## 4.3 The Tool Holder Shank

The tool holder shank that is used for the experimental procedures has a cross section of 32x25 mm. The geometry of the tool holder shank is presented in figure 4.1.

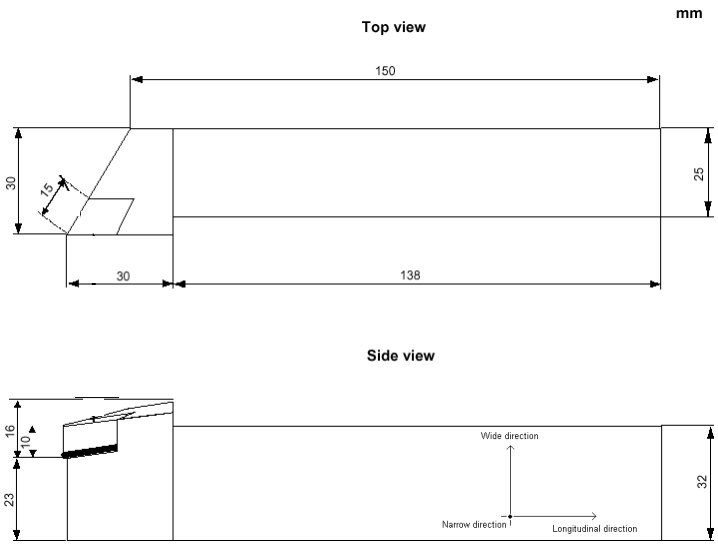


*Figure 4.1. The geometry of the tool holder shank.*

## 4.4 The Tool Holder Shank Free-Free

The first FE-model is built up with beam elements. It is important to get an apprehension of which frequencies the tool holder shank involves. The tool holder shank is built up with 7 elements and 8 nodes, see figure 4.2. Five elements with 32x25 mm, one with 36x26 mm and one with 30x12 mm cross section are used. The FE-model has 1 lumped mass of 0.020 kg. The mass of the FE-model is 1.26 kg and for the real tool holder shank 1.1 kg. The difference in mass between the FE-model and the experimental model depends among other things on the difficulty to achieve equal mass moment of inertia between the two models. Free-free boundary conditions for the tool holder shank are used and the eigenvalue problem is solved by the Lanczos method. The natural frequencies are presented in chapter 6 and the modeshapes are presented in Appendix A. A solid model for the tool holder shank is also created and presented in Appendix C.

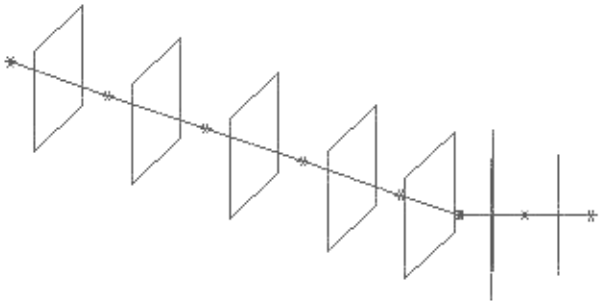

*Figure 4.2. The FE-model for the tool holder shank with beam elements and lumped mass.*

## 4.5 The Tool Holder and Tool Holder Shank Free-Free

### 4.5.1 With 40 mm Hang Out

The FE-model is built up with beam elements. The tool holder shank is built up with 5 elements and 6 nodes and 2 lumped masses, see figure 4.3. Three elements with 32x25 mm, one with 36x26 mm and one with 30x12 mm cross section are used. The FE-model has two lumped masses of 0.04 kg and 0.08 kg. To simulate the boundary conditions the FE-model is clamped at 40 mm hang out. The eigenvalue problem is solved by the Lanczos method. Results are presented in chapter 6.

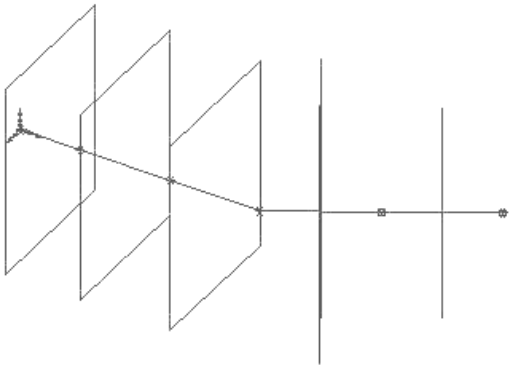

*Figure 4.3. The FE-model for the tool holder and tool holder shank free-free with beam elements and lumped masses.*

### 4.5.2 With 60 mm Hang Out

The FE-model is built up with beam elements. The tool holder shank is built up with 6 elements and 7 nodes and 2 lumped masses, see figure 4.4. Four elements of 32x25 mm, one with 36x26 and one with 30x12 mm cross section are used. The lumped masses are 0.02 kg and 0.01 kg. To simulate the boundary conditions the FE-model is clamped at 60 mm hang out. The eigenvalue problem is solved by the Lanczos method. Results are presented in chapter 6.

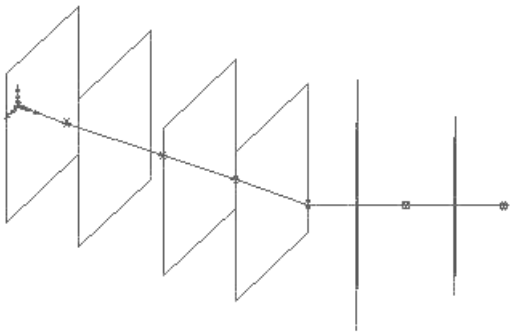

*Figure 4.4. The FE-model for the tool holder and tool holder shank free-free with beam elements and lumped masses.*

## 4.6 The Tool Holder and Tool Holder Shank in Concrete Lump

### 4.6.1 With 40 mm Hang Out

The FE-model is built up with beam elements. The tool holder shank is built up with 5 elements and 6 nodes and 2 lumped masses, see figure 4.3. Three elements of 32x25 mm, one with 36x26 and one with 30x12 mm cross section are used. The lumped masses in this case are 0.28 kg and 0.25 kg. To simulate the boundary conditions the FE-model is clamped at 40 mm hang out. The eigenvalue problem is solved by the Lanczos method. Results are presented in chapter 6.

### 4.6.2 With 60 mm Hang Out

The FE-model is built up with beam elements. The tool holder shank is built up with 6 elements and 7 nodes and 2 lumped mass, see figure 4.4. Four elements of 32x25 mm, one with 36x26 and one with 30x12 mm cross section are used. The lumped masses in this case are 0.35 kg and 0.3 kg. To simulate the boundary conditions the FE-model is clamped at 60 mm hang out. The eigenvalue problem is solved by the Lanczos method. Results are presented in chapter 6.

## 4.7 The Tool Holder and Tool Holder Shank in Lathe

### 4.7.1 With 40 mm Hang Out

The FE-model is built up with beam elements. The tool holder shank is built up with 5 elements and 6 nodes and 2 lumped masses, see figure 4.3. Three elements of 32x25 mm, one with 36x26 and one with 30x12 mm cross section are used. The lumped masses in this case are 0.3 kg and 0.2 kg. To simulate the boundary conditions the FE-model is clamped at 40 mm hang out. The eigenvalue problem is solved by the Lanczos method. Results are presented in chapter 6.

### 4.7.2 With 60 mm Hang Out

The FE-model is built up with beam elements. The tool holder shank is built up with 6 elements and 7 nodes and 2 lumped masses, see figure 4.4. Four elements of 32x25 mm, one with 36x26 and one with 30x12 mm cross section are used. The lumped masses in this case are 0.2 kg and 0.1 kg. To simulate the boundary conditions the FE-model is clamped at 60 mm hang out. The eigenvalue problem is solved by the Lanczos method. Results are presented in chapter 6.

# 5 Experimental Procedures

## 5.2 Excitation Methods and Requirements

The choice of experimental excitation method depends on several factors, such as the geometry and shape of the structure. It took several tests to establish a method to use for our application. The structure could be excited either by an impulse hammer or by using a shaker connected with an impedance head by a flexible drive rod, see figure 5.1. The impulse hammer gives rise to an impulse signal when exciting the structure with a distinct shock. The shaker gives rise to a vibrating excitation signal that is transferred into the structure by an impedance head. The impedance head is a force transducer and an accelerometer in one; it measures the acceleration and the input force in the same point, the so-called driving point.

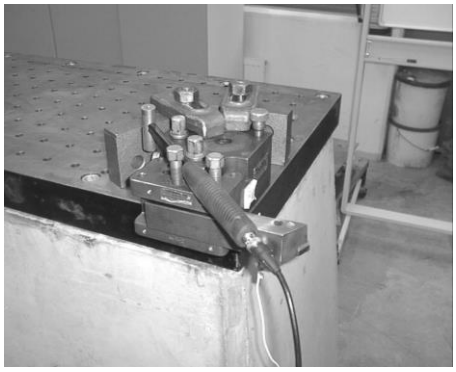

a)

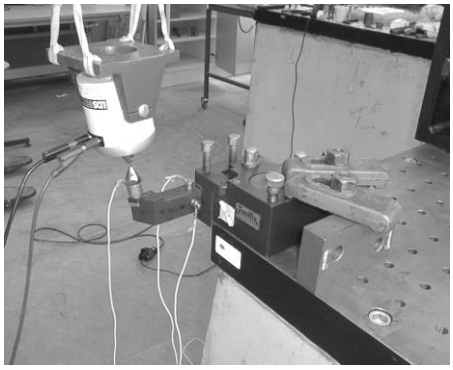

b)

*Figure 5.1. Two excitation methods, a) impulse hammer excitation and b) shaker excitation.*

The requirements for the excitation method were that the frequency range amount to 12.8 kHz and that sufficient energy are still in the system at least up to 10 kHz. These requirements were thought to be fulfilled by both excitation methods at the beginning, but after several tests it came clear that the shaker excitation only has sufficient energy up to approximately 4 kHz. The problems when measuring with the shaker is that it is very important to mount the impedance head in the centre of the tool holder shank to avoid

undesired movements and moments into the structure. Another problem is the mass spring system of the impedance head that could affect the natural frequencies of the system. These facts excluded the shaker as excitation method.

## 5.3 Equipment in All Experimental Measurements

The following equipment is used, Hewlett Packard measuring system HP-3565S, impulse hammer PCB with force sensor PCB model 086C03, nickel tip and I-DEAS test software v.5.

## 5.4 The Tool Holder Shank Free-Free

The following equipment is used, tool holder shank, two accelerometers Dytran model 3220A, Loctite fast glue as adhesive for mounting the accelerometers, rubber bands and hoop.

The tool holder shank is mounted with rubber bands on the hoop to isolate it from disturbance from the surroundings, see figure 5.2.

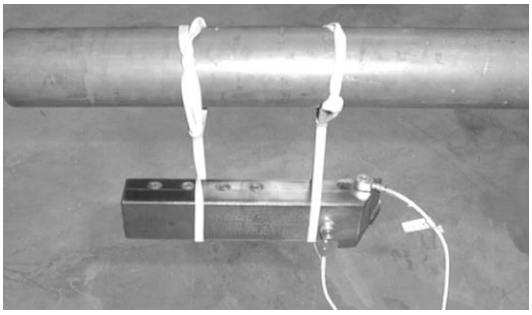

*Figure 5.2. Experimental set-up for the tool holder shank free-free.*

The accelerometers are mounted in two directions (wide and narrow) at the planar surfaces at the front end of the tool holder shank, see figure 5.3. Excitation is done with the impulse hammer in the points of interest, and perpendicular to the surface of the tool holder shank.

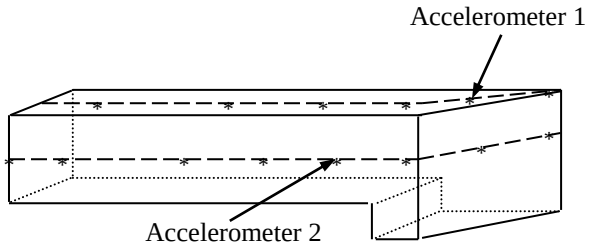


*Figure 5.3. Measuring points and accelerometers placements.*

Nodes and trace lines are created in I-DEAS test Modal preparation for the measuring points, see figure 5.4a and b. The two nodes at the front end side, where the surface is leaning are connected to a local co-ordinate system. The other nodes are connected to the global co-ordinate system.


*Figure 5.4a. Tracelines for the tool holder shank, seen from above.*

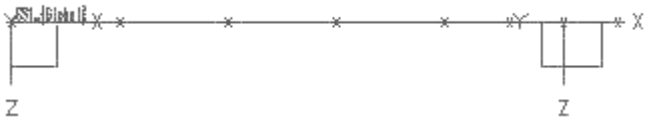


*Figure 5.4b. Tracelines for the tool holder shank, seen from beside.*

## 5.5 The Tool Holder and Tool Holder Shank Free-Free

The following equipment is used: tool holder, tool holder shank, two accelerometers Dytran model 3220A, Loctite fast glue as adhesive for mounting the accelerometers, rubber bands and hoop.

The tool holder shank is attached to the tool holder with two screws with a tightening moment of 100 Nm and treated as one structure. The structure is mounted with rubber bands on the hoop to isolate it from disturbance from the surroundings, see figure 5.5.

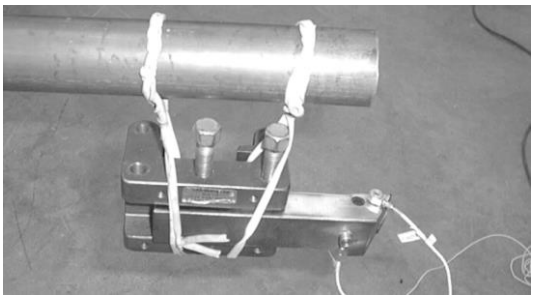

*Figure 5.5. Experimental set-up for the tool holder and tool holder shank free-free.*

The measurement is done twice for different mounting lengths of the tool holder shank. First for 40 mm, second for 60 mm.

The accelerometers are mounted as in figure 5.3. Excitation is done with the impulse hammer in the points of interest, and perpendicular to the surface of the tool holder shank. The two nodes at the front end side, where the surface is leaning are connected to a local co-ordinate system. The other nodes are connected to the global co-ordinate system, see figure 5.6 and figure 5.7.

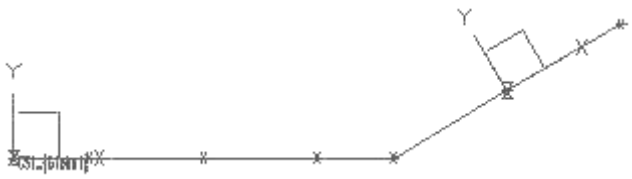

*Figure 5.6a. Tracelines for the tool holder shank. 40 mm hang out , seen from above.*

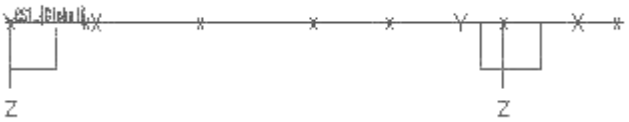

*Figure 5.6b. Tracelines for the tool holder shank, 40 mm hang out, seen from beside.*

*Figure 5.7a. Tracelines for the tool holder shank, 60 mm hang out, seen from above.*

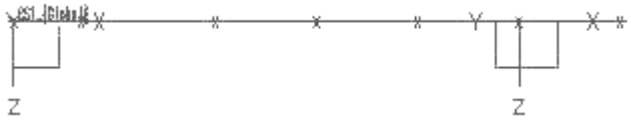

*Figure 5.7b. Tracelines for the tool holder shank, 60 mm hang out, seen from beside.*

## 5.6 The Tool Holder and Tool Holder Shank in Concrete Lump

### 5.6.1 Measurements with Accelerometers

The following equipment is used, tool holder, tool holder shank, tool holder attachment, two accelerometers Dytran model 3220A, Loctite fast glue as adhesive for mounting the accelerometers and maintaining their physical properties and fastening elements.

The tool holder shank is attached to the tool holder with two screws. The complete structure is then fastened into the concrete lump with fastening elements trying to simulate the lathe to minimise the disturbances acting on

the tool holder shank when in the lathe. The accelerometers are mounted as in figure 5.3. Excitation is done with the impulse hammer in the points of interest, and perpendicular to the surface of the tool holder shank. Nodes, trace lines and co-ordinate systems are created as in section 5.5. The measurement is done twice for different mounting lengths of the tool holder shank. First for 40 mm, second for 60 mm. The tightening moments $M_t$ that is used for tightening the fastening elements is chosen to 100, 120 and 140 Nm, see Figure 5.8.

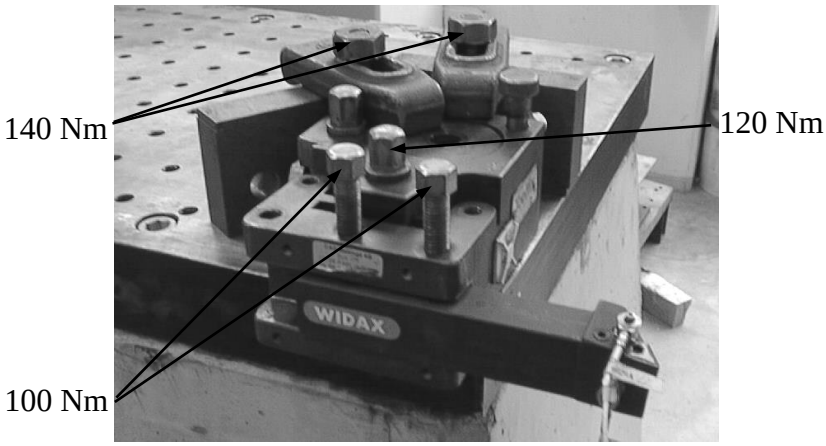


*Figure 5.8. Experimental set-up for the tool holder and tool holder shank in concrete lump.*

### 5.6.2 Measurements with Laser Vibrometer

The following equipment is used: tool holder, tool holder shank, tool holder attachment, oscilloscope, laser vibrometer VS-100 with power supply and fastening elements.

The tool holder shank is attached to the tool holder with two screws. The complete structure is then fastened into the concrete lump with fastening elements trying to simulate the lathe to minimise the disturbances acting on the tool holder shank when in the lathe. The laser beam is directed into the tool holder shank measuring the velocity when an impulse is made with the impulse hammer. The distance from the laser vibrometer to the structure is 830 mm, which is one of the optimum distances recommended from the manual of the laser vibrometer, see figure 5.9. The measuring points are the

same as in section 5.5. Excitation is done with the impulse hammer in the points of interest, and perpendicular to the surface of the tool holder shank. Nodes, trace lines and co-ordinate systems are created as in section 5.5. The measurement is done twice for different mounting lengths of the tool holder shank. First for 40 mm, second for 60 mm.

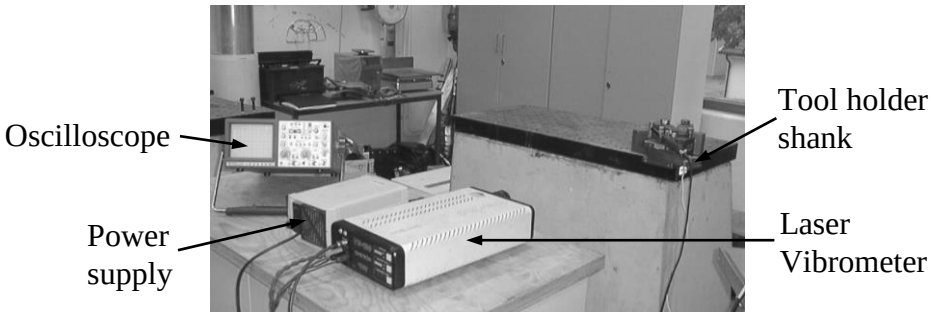


*Figure 5.9. Experimental set-up for the tool holder and tool holder shank in concrete lump.*

## 5.7 The Tool Holder and Tool Holder Shank in Lathe

The following equipment is used, tool holder, tool holder shank, lathe, two accelerometers Dytran model 3220A, Loctite fast glue as adhesive for mounting the accelerometers and maintaining their physical properties, oscilloscope, laser vibrometer VS-100 with power supply.

The tool holder shank is placed in the tool holder and fixed into the lathe. Measurements are made first with two accelerometers and second with the laser vibrometer for the mounting lengths of 40 and 60 mm for the tool holder shank, see figure 5.10 and figure 5.11. The distance used for the Laser vibrometer in this case is 220 mm, recommended from the manual.

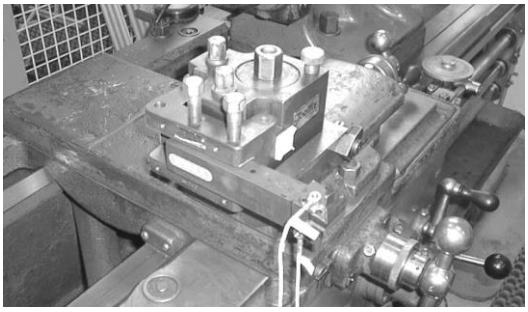

*Figure 5.10. Experimental set-up for the tool holder and tool holder shank in lathe with accelerometers.*

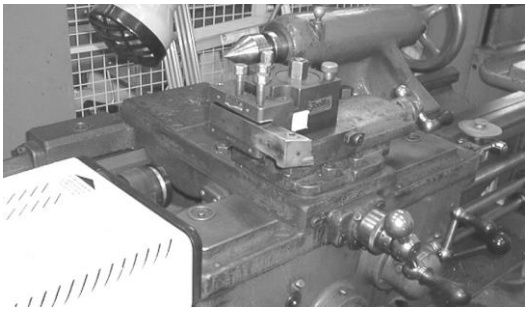

*Figure 5.11. Experimental set-up for the tool holder and tool holder shank in lathe with laser vibrometer.*

# 6 Results

The modes that are interesting are the bending modes in the wide and narrow direction, see figure 4.1. The theoretical and experimental results of the frequencies for the tool holder and tool holder shank are presented in tables 6.1 – 6.8 below. The mode shapes for the tool holder shank free-free are presented in Appendix A, the comparison of natural frequencies and modeshapes are presented in Appendix B.

*Table 6.1. Results for the tool holder shank free-free with accelerometers.*

| **Mode Number** | **FE-Results beam elements Frequency (Hz)** | **Experimental Results Frequency (Hz)** | **Difference between FE. and Exp. (%)** | **Damping ratio (%)** |
|---|---|---|---|---|
| 1 | 4503 | 4503 | 0 | 0.29 |
| 2 | 5567 | 5479 | 1.6 | 0.39 |
| 3 | 10905 | 10646 | 2.4 | 0.39 |

*Table 6.2. Results for the tool holder and tool holder shank free-free, 40 mm hang out with accelerometers.*

| **Mode Number** | **FE-Results beam elements Frequency (Hz)** | **Experimental Results Frequency (Hz)** | **Difference between FE. and Exp. (%)** | **Damping ratio (%)** |
|---|---|---|---|---|
| 1 | 2956 | 2798 | 5.6 | 0.27 |
| 2 | 3568 | 3685 | 3.3 | 0.80 |
| 3 | 10484 | 11112 | 6.0 | 0.47 |

*Table 6.3. Results for the tool holder and tool holder shank free-free, 60 mm hang out.*

| Mode Number | FE-Results beam elements Frequency (Hz) | Experimental Results Frequency (Hz) | Difference between FE. and Exp. (%) | Damping ratio (%) |
|---|---|---|---|---|
| 1 | 2385 | 2362 | 1.0 | 0.33 |
| 2 | 2927 | 3080 | 5.2 | 0.28 |
| 3 | 10015 | 9165 | 9.3 | 0.37 |

*Table 6.4. Results for the tool holder and tool holder shank in concrete lump, 40 mm hang out with accelerometers.*

| Mode Number | FE-Results beam elements Frequency (Hz) | Experimental Results Frequency (Hz) | Difference between FE. and Exp. (%) | Damping ratio (%) |
|---|---|---|---|---|
| 1 | 1789 | 1856 | 3.7 | 1.69 |
| 2 | 2145 | 2072 | 3.5 | 0.81 |
| 3 | - | - | - | - |

*Table 6.5. Results for the tool holder and tool holder shank in concrete lump, 60 mm hang out with accelerometers.*

| Mode Number | FE-Results beam elements Frequency (Hz) | Experimental Results Frequency (Hz) | Difference between FE. and Exp. (%) | Damping ratio (%) |
|---|---|---|---|---|
| 1 | 1109 | 1096 | 1.2 | 0.95 |
| 2 | 1365 | 1340 | 1.9 | 0.86 |
| 3 | - | - | - | - |

*Table 6.6. Results for the tool holder and tool holder shank in lathe, 40 mm hang out with accelerometers.*

| Mode Number | FE-Results beam elements Frequency (Hz) | Experimental Results Frequency (Hz) | Difference between FE. and Exp. (%) | Damping ratio (%) |
|---|---|---|---|---|
| 1 | 1868 | 1776 | 5.2 | 0.82 |
| 2 | 2239 | 2336 | 4.3 | 0.94 |
| 3 | - | - | - | - |

*Table 6.7. Results for the tool holder and tool holder shank in lathe, 60 mm hang out with accelerometers.*

| Mode Number | FE-Results beam elements Frequency (Hz) | Experimental Results Frequency (Hz) | Difference between FE. and Exp. (%) | Damping ratio (%) |
|---|---|---|---|---|
| 1 | 1497 | 1264 | 18.4 | 0.62 |
| 2 | 1903 | 2032 | 6.8 | 0.58 |
| 3 | - | - | - | - |

*Table 6.8. Results for the tool holder and tool holder shank in concrete lump and lathe, 40 and 60 mm hang out with laser vibrometer.*

| Experimental Results Frequency (Hz) | | | | |
|---|---|---|---|---|
| Mode Number | 40 mm hang out in concrete lump | 60 mm hang out in concrete lump | 40 mm hang out in lathe | 60 mm hang out in lathe |
| 1 | 1712 | 1216 | 1712 | 1232 |
| 2 | 1760 | 1592 | 2080 | 2112 |
| 3 | - | - | - | - |

# 7 Conclusions

The aim of this work was to determine the natural frequencies, mode shapes and damping ratios for a tool holder shank. This is considered to be a suitable first step in investigating if it would be possible to use piezoelectric actuators to reduce vibrations during the cutting process. Finite element models to describe the tool holder shank have been suggested. Agreement, disagreement, and possible reasons for disagreement between results predicted by these models and by experimental measurements are discussed below.

There is no single right way to perform a vibration test. In almost every case the support, the excitation equipment or the transducers will influence the dynamic behaviour of a structure under an experimental test. It is very important to realise these influences, understand them and design the test to minimise their effects on the dynamic behaviour of the structure. All modal tests involve a degree of compromise. Almost all methods for applying the structural excitation will have some unwanted modification on the structure. Similarly almost all the response measurement transducers and support fixtures will have unwanted influence on the structure.

## 7.1 Complexity of Problems

It is very important to get the right set-up for the experimental procedure to have good agreement between the experiment and the FE-model. It is also very important to get the right boundary conditions. The problem is to define how the tool holder and tool holder shank are fixed together. Consideration of the support of the structure under test is an important part of the test set-up. The support conditions should be well defined and experimentally repeatable. It is almost impossible to achieve a complete grounded structure in practice. A grounded structure will have some movement at the grounding point, usually rotation.

The agreement between the experimental and the FE-calculated frequencies for the tool holder shank free-free is good. Also for the tool holder and tool holder shank free-free there is good agreement.

The modeshapes of the experimental model and the FE-model for the tool holder shank free-free agree well, except for the nodes beside the measuring points were the accelerometers are mounted, because no excitation is made in these points.

The agreement between the experimental and the FE-calculated frequencies for the tool holder and tool holder shank in concrete lump and lathe is not so good. The problem is to decide which frequencies really are frequencies belonging to the tool holder shank. A reason among others is that the stiffness between the tool holder and the tool holder shank is much lower than the stiffness of the tool holder and the tool holder shank itself.

Another problem is that the distance *L1* and *L2* are different, see figure 7.1. When the tool holder shank moves in the negative *y*-direction the length is *L1*. When it moves in the positive *y*-direction the length is *L2*. That means that we have two linear systems. One for length *L1*, and one for length *L2*. Together they build a non-linear system depending on its position. When it moves in the positive *y*-direction the length varies from *L1* to *L2*, which means that the movement between *L1* and *L2* is non-linear depending on its position, see figure 7.1 and 7.2. This will result in two different frequencies during its movements from its negative to its positive direction. This problem will also come up in the *z*-direction (perpendicular to the paper). This is one reason for the less good agreement between the experimental and the theoretical frequencies and mode shapes.

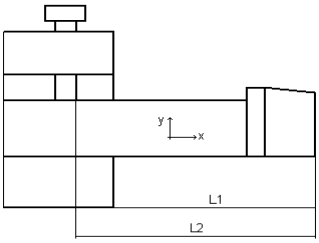


*Figure 7.1. The tool holder and tool holder shank with length L1 and L2.*

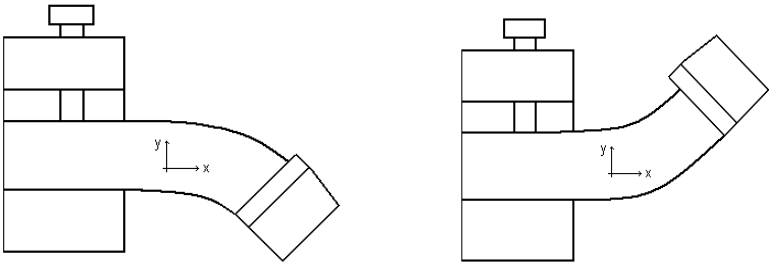


*Figure 7.2. The tool holder and tool holder shank bending in the negative and positive y-direction.*

The tightening moment $M_t$ also affects the frequencies. The moment that is used in the experiment is 100, 120 and 140 Nm for the five bolts, see figure 5.6. A comparison is done between two different tightening moments $M_t$. ADF number 32 is tightened with 100, 120 and 140 Nm and the ADF number 48 is tightened with 60, 80 and 140 Nm, see figure 7.3. The tightening tool has also a source of error of about 5-10 %.

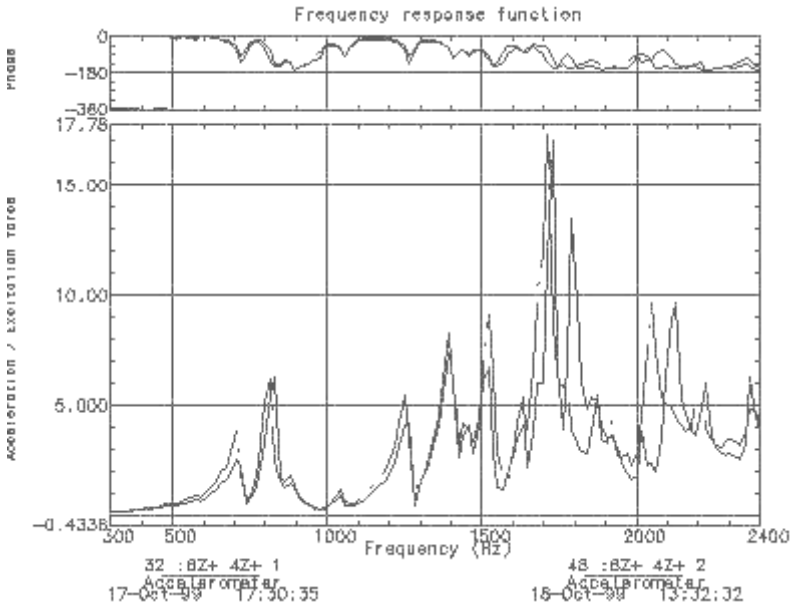


*Figure 7.3. FRF for different tightening moments $M_t$.*

The lathe has a lot of parts that also have natural frequencies. The attachment for the tool holder, as the screws on the attachment for the tool

holder, also has natural frequencies. A great problem is to decide which frequencies that really are frequencies belonging to the tool holder shank.

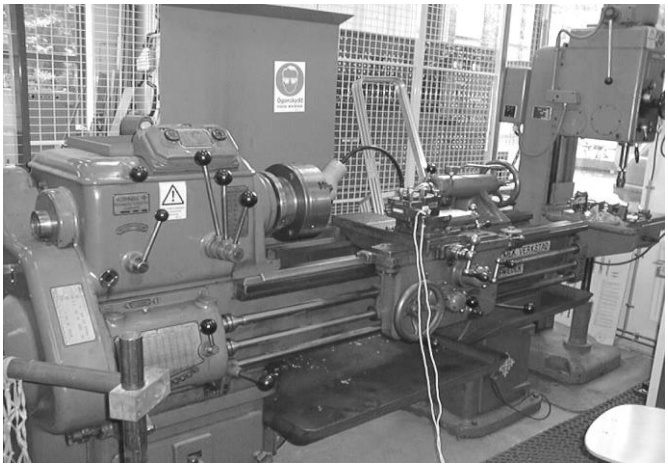

*Figure 7.4. The lathe with the tool holder and tool holder shank.*

Accelerometers build in new mass/spring systems that could affect the natural frequencies of the tool holder shank.

The problems mentioned makes it difficult to determine the natural frequencies for the tool holder and tool holder shank in concrete lump and in lathe. In Appendix D FRFs from measurements with the laser vibrometer for the tool holder shank in concrete lump is presented. One reason for the poor measurements can be the problem for the laser to register the high velocities for frequencies from 5000 Hz and up.

Getting correct modal data from relatively complex structures involves many difficulties. A minority of measurement points may probably not indicate some of the mode shapes. But increasing the number of locations not only increase the time of experiment but also induce more errors, such as noise, improper positioning of the impulse hammer and exciter, signal truncation error due to selection of window, and so forth.

## 7.2 The Continuation of the Analysis of the Tool Holder Shank

With the basic knowledge of the dynamic characteristics of the tool holder shank obtained in this work the next step would be to include actuators in the model. The actuators can perhaps be modelled as forces/pressures on the two surfaces, according to figure 7.5. The voltage to the actuators could be controlled from for example a Matlab-Simulink routine. By modelling the tool holder shank in Femlab the whole system could be simulated in the same software. Doing this would give an idea of how much the dynamic behaviour of the tool holder shank can be influenced by actuators.

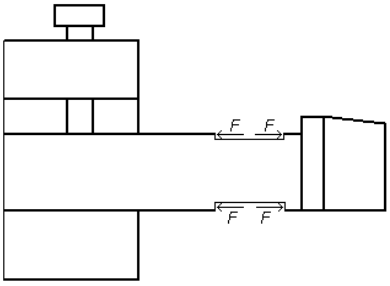


*Figure 7.5. Simulation of the actuators.*

# 8 References


1. Andersson, P., *Anordning för vibrationsassisterad bearbetning i supportsvarv*, MSc Thesis, Lund, 1990.
2. Björklund, S., Hågeryd, L., Lenner, L., *Modern Produktions Teknik Del 1*, Liber Utbildning, 1993.
3. Craig, Jr., Roy, R., *Structural Dynamics, an Introduction to Computer Methods*, John Wiley & Sons, 1981.
4. Ewins, D.J., *Modal Testing: Theory and Practice*, Research Studies Press Ltd., 1984.
5. Golub, G.H., Van Loan, C.F., *Matrix computations*, The Johns Hopkins University Press, 1989.
6. Håkansson, L., *Adaptive Active Control of Machine – Tool Vibration in a Lathe*, PhD Thesis, KFS AB Lund, 1999.
7. Inman, D.J., *Engineering Vibration*, Prentice-Hall, Inc., 1996.
8. Maia, Silva, He, Lieven, Lin, Skingle, To, Urgueira, *Theoretical and Experimental Modal Analysis*, Research Studies Press Ltd, 1997.
9. Newland, D.E., *Random Vibrations, Spectral Wavelet Analysis*, Longman Singapore Publishers Pte Ltd, 1993.
10. PCB Piezotronics, *AVC Instrumentation*, http://www.pcb.com/products/avc/avc713a01.html, 1999-07-12
11. Philips, *Piezoelectric Ceramics Properties And Applications*, N. V. Philips´ Gloeilampenfabrieken, 1991.

# Appendix A

*Figure A.1. The first mode for the tool holder shank free-free with beam elements.*

*Figure A.2. The second mode for the tool holder shank free-free with beam elements.*

*Figure A.3. The third mode for the tool holder shank free-free with beam elements.*

*Figure A.4. The first experimental mode for the tool holder shank free-free.*

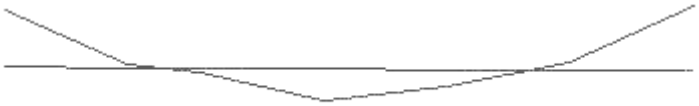

*Figure A.5. The second experimental mode for the tool holder shank free-free.*

*Figure A.6. The third experimental mode for the tool holder shank free-free.*

# Appendix B

*Figure B.1. Measured versus predicted natural frequencies for the tool holder shank free-free.*

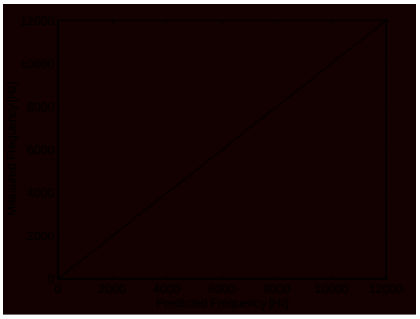

*Figure B.2. Measured versus predicted natural frequencies for the tool holder and tool holder shank free-free, 40 mm hangout.*

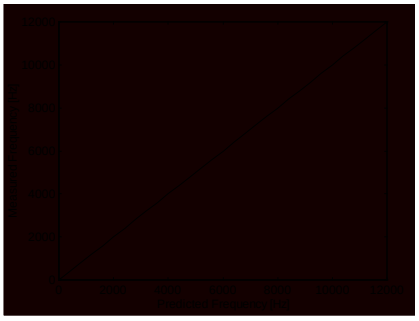

*Figure B.3. Measured versus predicted natural frequencies for the tool holder and tool holder shank free-free, 60 mm hangout.*

*Figure B.4. Traceline and nodes for the tool holder shank free-free, seen from above.*

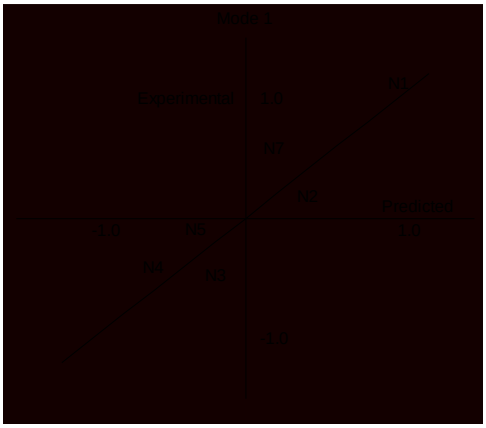


*Figure B.5. Comparison of mode shape 1 for the tool holder shank free-free, experimental versus predicted.*

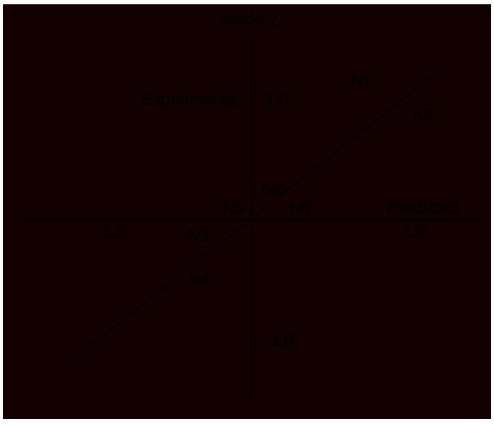


*Figure B.6. Comparison of mode shape 2 for the tool holder shank free-free, experimental versus predicted.*

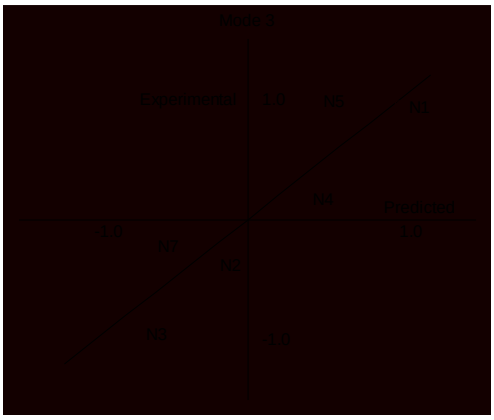


*Figure B.7. Comparison of mode shape 3 for the tool holder shank free-free, experimental versus predicted.*

# Appendix C

### The FE-model for the Tool Holder Shank Free-Free with Solid Elements

The tool holder shank is modelled as a solid part spliced into two parts, see figure C.1. The reason for splicing the solid model in two parts is to mesh the two different parts with different mapped mesh.

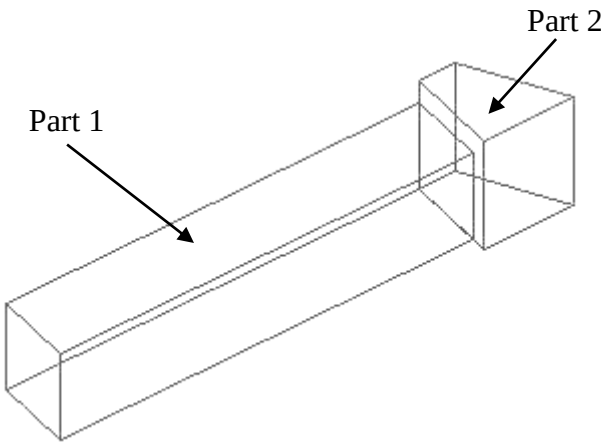


*Figure C.1. The tool holder shank modelled in two parts.*

Part 1 is meshed with 23 elements in longitudinal direction, 8 elements in the wide direction and 5 elements in the narrow direction, see Figure C.2. Part 2 is meshed with 4 elements in the longitudinal, 10 elements in the wide and 6 elements in the narrow direction. The total number of elements is 1240 and the total number of nodes is 1735.

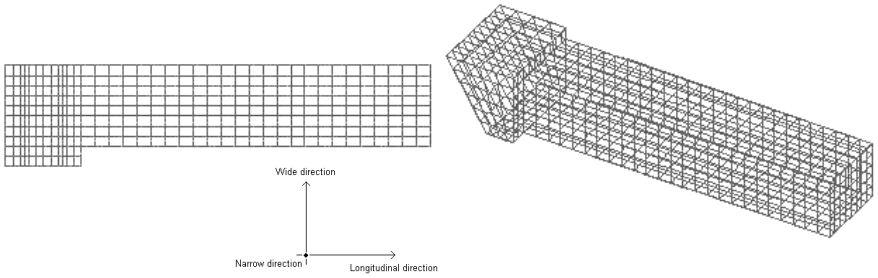


*Figure C.2. The mesh of the tool holder shank in longitudinal, wide and narrow direction.*

The mass of the tool holder shank in the FE-model is 1.06 kg. The boundary conditions for the tool holder shank is free-free and the eigenvalue problem is solved by the Lanczos method. Results see Figure C.3-C.5.

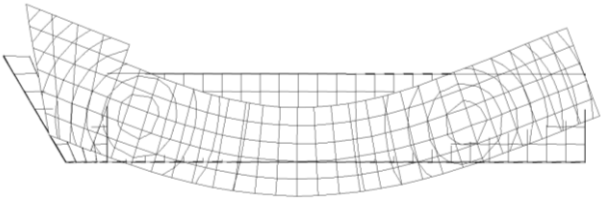

*Figure C.3. The first mode for the tool holder shank free-free with solid elements.*

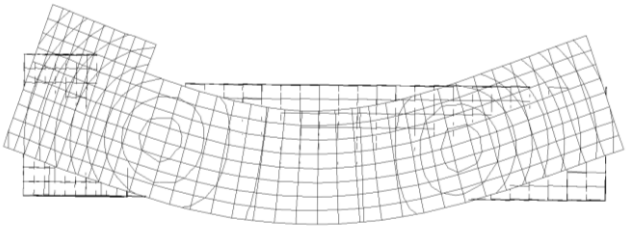

*Figure C.4. The second mode for the tool holder shank free-free with solid elements.*

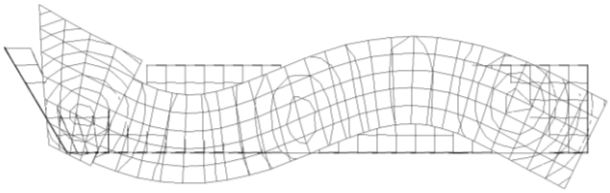

*Figure C.5. The third mode for the tool holder shank free-free with solid elements.*

# Appendix D

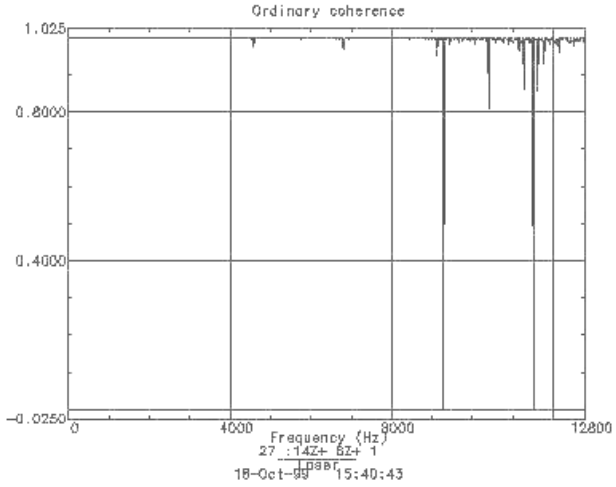


*Figure D.1. Coherence function for the FRF below.*

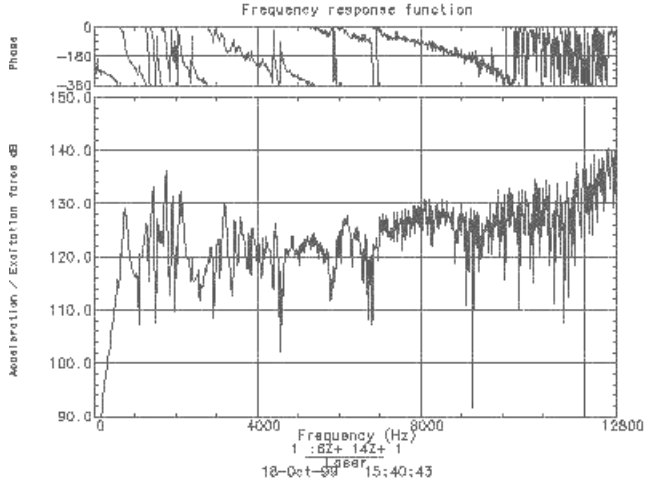


*Figure D.2. Accelerance FRF for the tool holder and tool holder shank in concrete lump.*

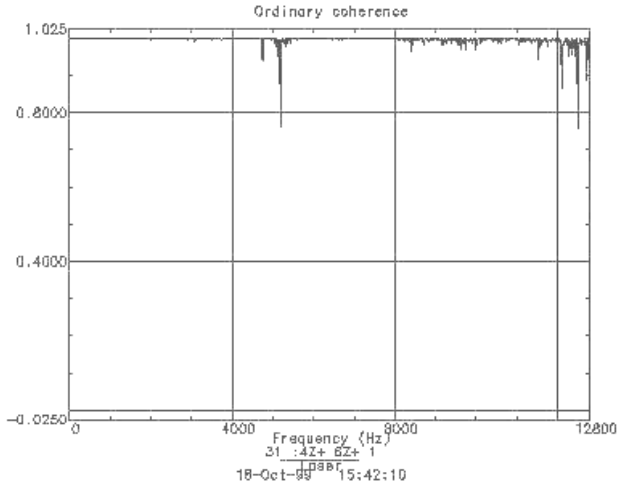


*Figure D.3. Coherence function for the FRF below.*

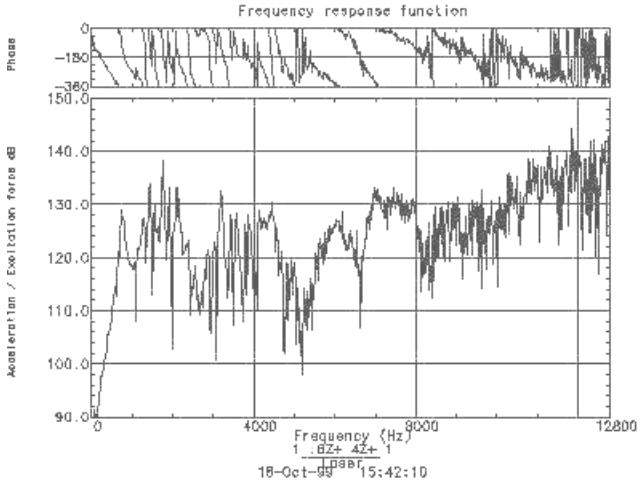


*Figure D.4. Accelerance FRF for the tool holder and tool holder shank in lathe.*